Asymptotic profiles for a travelling front solution of a biological equation

Guillemette CHAPUISAT* & Romain JOLY†

May 27, 2011

Abstract

We are interested in the existence of depolarization waves in the human brain. These waves propagate in the grey matter and are absorbed in the white matter. We consider a two-dimensional model $u_t = \Delta u + f(u)\mathbb{1}_{|y|\leq R} - \alpha u \mathbb{1}_{|y|>R}$, with f a bistable nonlinearity taking effect only on the domain $\mathbb{R} \times [-R, R]$, which represents the grey matter layer. We study the existence, the stability and the energy of non-trivial asymptotic profiles of the possible travelling fronts. For this purpose, we present dynamical systems techniques and graphic criteria based on Sturm-Liouville theory and apply them to the above equation. This yields three different types of behaviour of the solution u after stimulation, depending on the thickness R of the grey matter. This may partly explain the difficulties to observe depolarisation waves in the human brain.

Keywords: spreading depression, reaction-diffusion equation, travelling fronts, Sturm-Liouville theory.

AMS classification codes (2000): 34C10, 35B35, 35K57, 92C20.

1 Introduction

The propagation of depolarisation waves, also called cortical spreading depressions, may appear in a brain during strokes, migraines with aura or epilepsy. In rodent brains, the propagation of depolarisation waves has been observed for more than fifty years [17]. During stroke in rodent brain, they cause important damages and are therefore a therapeutic target. Pharmacological agents blocking the appearance of those waves have been studied and reduce strongly after-effects of stroke in the rodent brain [20, 21]. However propagation of depolarisation waves during stroke in the human brain is still uncertain [1, 18, 19, 29, 30] and the pharmacological agents used in rodent have seemed to have no

*Université Paul Cézanne, CNRS, LATP (UMR 6632), Faculté des Sciences et Techniques de St Jérôme, Case Cour A, av Escadrille Normandie-Niemen, 13397 Marseille Cedex 20, France. guillemette.chapuisat@univ-cezanne.fr

†Institut Fourier, UMR 5582 CNRS/Université de Grenoble, 100, rue des maths, BP 74, 38402 Saint-Martin-d'Hères, France. romain.joly@ujf-grenoble.fr

effect on human stroke. Most experiments on those waves in human brain are impossible for ethical or technical reasons but mathematical models and their analysis may help to understand these points.

A parabolic model for spreading depression. Depolarisation waves are consequence of ionic perturbations in the brain. They result from complicate reactions (opening of various ionic channels and inversion of different ionic transporters on the cell membrane) at the cellular level in the grey matter and of diffusion of ions in the extracellular space. After several minutes, the cells of the grey matter repolarize and another wave can be created. In the white matter, ions can diffuse but no reaction takes place since there is no neuronal soma. Several models of depolarisation wave have already been established [23, 24, 27, 31]. They focus on how those waves are triggered and/or on their consequences on the brain tissue. They are set on a homogeneous one or two dimensional space and mainly represent the situation in the grey matter of a rodent brain. Mathematical proofs of existence of travelling waves for such models in the grey matter of a brain have been established [32]. Here we want to investigate the discrepancies between human and rodent that may explain the difficulties to observe these waves during stroke in human and we specially focus on the influence of the white matter of the human brain on the propagation of these waves. The spreading depression are created in the grey matter and absorbed in the white matter, therefore one expects that the geometry of both layers may explain the existence or not of depolarisation waves. We are not interested in the repolarisation phenomena, hence we will not include it in our model.

In [3], the first author has already built a mathematical model of these waves and has studied numerically how the brain morphology may influence their propagation. In this model, the function u represents the depolarisation of the brain in such a way that if $u(X) = 0$ the brain is normally polarised at the point X whereas if $u(X) = 1$ the brain is totally depolarised. The simplest equation to model depolarisation waves is a bistable reaction-diffusion in the grey matter while in the white matter, the depolarisation diffuses and is progressively absorbed. Hence the study of existence of depolarisation wave in the human brain leads to the following biological equation

$$\frac{\partial u}{\partial t} - \triangle u = f(u)\mathbb{1}_{\Omega} - \alpha u \mathbb{1}_{\mathbb{R}^N \setminus \Omega}, \qquad t \in \mathbb{R},\, X \in \mathbb{R}^N, \tag{1.1}$$

where $f(u) = \lambda u(u-a)(1-u)$ is the usual bistable nonlinearity with $a \in]0, 1/2[$ and $\lambda > 0$, and where α is a positive number. We denote by $\mathbb{1}_{\Omega}$ the characteristic function of the domain Ω that is $\mathbb{1}_{\Omega}(X) = 1$ if $X \in \Omega$ and $\mathbb{1}_{\Omega}(X) = 0$ elsewhere. The domain Ω represents the grey matter of a brain, where the reaction-diffusion process that triggers depolarisation waves takes place, whereas $\mathbb{R}^N \setminus \Omega$ contains the white matter, where the waves are absorbed.

A depolarisation wave corresponds to a travelling front where a nonzero state invades the zero state. The problem is to understand the influence of the geometry of Ω on the propagation of waves. In particular, the layer of grey matter in the human brain is thinner than in other species and admits more circumvolutions. The influence of the circumvolutions of the grey matter is partially studied in [5, 22]. There, we assume that Ω is a straight cylinder of radius R and we focus on the influence of the parameter R. Indeed, it appeared that the thickness of the grey matter layer in the human brain has a crucial

importance. In [3], numerical studies have shown that small values of R may prevent the spreading of the ionic waves. A partial theoretical study in any dimension N has been led in [4], where the first author has proved the nonexistence of the depolarisation waves if the thickness R is small enough and their existence if R is large enough. The results of [4] are not completely satisfactory. First, they only deal with R small or large enough. Secondly, no complete description of the possible asymptotic profiles of the travelling waves, their stability, or their energy, has been pursued. As a consequence, even if the existence of waves is proved, nothing is known about their asymptotic profiles and their stability. In the present paper, we complete this study for any R, in dimension $N = 2$.

The dynamics of the parabolic equation on a segment. Eq. (1.1) is a parabolic reaction-diffusion equation. The qualitative dynamics of parabolic equations are an important subject of research. In particular, the dynamics of the one-dimensional scalar parabolic equation on a segment,

$$\frac{\partial u}{\partial t}(y,t) = \frac{\partial^2 u}{\partial y^2}(y,t) + g\big(y, u(y,t), \frac{\partial u}{\partial y}(y,t)\big) \quad , \quad (y,t) \in (0,1) \times \mathbb{R}_+ \ . \tag{1.2}$$

with either Dirichlet, Neumann or Robin boundary conditions, are now well understood. The study of the dynamics of (1.2) began with Chafee-Infante equation [2]. Fusco and Rocha have shown in [9] how several informations, as for example the stability of equilibrium points, can be read from the phase plane. One of the main tools of these papers is Sturm-Liouville theory and Sturm theorem, which are specific to the one-dimensional parabolic equation. Using these properties and general techniques coming from the study of dynamical systems, one is able to describe completely the dynamics of (1.2), see [7] and the reference therein. Several reviews exist on this subject, see for example [8].

To our knowledge, the techniques developed for understanding the dynamics of Eq. (1.2) have rarely been applied in concrete modelling problems. Articles as [9] or [7] are motivated by the beauty of their theoretical results. We show here that these techniques can be applied to obtain a better understanding of concrete problems.

Main results. We consider the equation

$$\frac{\partial u}{\partial t} = \triangle u + f(u)\mathbb{1}_{|y|\leq R} - \alpha u \mathbb{1}_{|y|>R}, \qquad t \in \mathbb{R},\, (x,y) \in \mathbb{R}^2 \ . \tag{1.3}$$

It corresponds to a two-dimensional version of (1.1) where the grey matter forms a layer of thickness $2R$. Of course, it also describes the behaviour of solutions independent of z for a three-dimensional model with a grey matter lying in a planar layer.

We are looking for solutions travelling in the x direction at speed c, that are solutions u of (1.3) which can be written $u(x,y,t) = v(x-ct,y)$. Travelling fronts are solutions $u(x,y,t) = v(x-ct,y)$ such that there are two asymptotic profiles $V_- \neq V_+$ with $\lim_{\xi\to\pm\infty} \|v(\xi,.) - V_\pm\|_{H^1(\mathbb{R})} = 0$. Using standard elliptic estimates, a profile V is a solution in $H^1(\mathbb{R})$ of the equation

$$V'' + f(V)\mathbb{1}_{|y|\leq R} - \alpha V \mathbb{1}_{|y|>R} = 0, \quad y \in \mathbb{R} \ , \tag{1.4}$$

that is a stationary point of

$$\frac{\partial v}{\partial t}(y,t) = \frac{\partial^2 v}{\partial y^2}(y,t) + f(v(y,t))\mathbb{1}_{|y|\leq R} - \alpha v(y,t)\mathbb{1}_{|y|>R} = 0, \quad (y,t) \in \mathbb{R}\times\mathbb{R}_+ \,. \qquad (1.5)$$

Notice that a profile is trivially associated to an equilibrium point $E(x,y) = V(y)$ that is a stationary solution of (1.3). The trivial equilibrium point $E \equiv 0$ corresponds to the normal state of the brain, whereas a non-trivial equilibrium point corresponds to a depolarised state, deleterious for the brain. We are more particularly interested in the existence of travelling fronts with positive speed c connecting the profile $V_+ \equiv 0$ with a non-trivial profile V_-. Such fronts correspond to the invasion of the equilibrium state 0 by a deleterious state.

In this article, we achieve a complete study of the existence of the profiles of (1.4), of their stability and their energy (see the following sections for the definitions of stability and energy). Precisely, the following theorem will be proved.

Theorem 1.1. *There exist two critical thicknesses $R_1 > R_0 > 0$ such that:*
i) if $0 < R < R_0$, there is no non-trivial profile, i.e. that $V \equiv 0$ is the only solution of (1.4) in $H^1(\mathbb{R})$.
ii) If $R_0 < R$, there exist non-trivial profiles. One of them, denoted by V_M, is larger than every other one. The largest profile V_M is stable, and every other non-trivial profiles are unstable.
iii) The energy of the unstable profiles is always larger than the energy of the stable profiles 0 and V_M. If $R_0 < R < R_1$, the energy of V_M is larger than the energy of 0, whereas it is smaller if $R > R_1$.

For proving this theorem, we use ideas coming from the study of dynamics of PDE, in particular of the parabolic equation on a segment. Sturm-Liouville theory and the ideas of [9] are adapted to Eq. (1.5) to establish the stability of the profiles. The study of the energy of the profiles is based on proving the existence of heteroclinic connections between profiles. Both proofs are based on general dynamical techniques and on graphic criteria, which are valid for any nonlinearity f. We obtain the above results by applying these ideas to the particular nonlinearity $f(u) = \lambda\ u(u-a)(1-u)$. The check on the graphic criteria sometimes relies on a numerical study of the phase plane.

Three types of qualitative behaviour. Once the profiles and their stability completely described by Theorem 1.1, one is able to obtain the existence of travelling fronts.

Consequences 1.2.
i) If $0 < R < R_0$ then there is no travelling front for Eq. (1.3).
ii) If $R_0 < R < R_1$ there exists a globally stable travelling front $u(x,y,t) = v(x-ct,y)$ with $\lim_{\xi\to+\infty} v(\xi,.) = 0$ and $\lim_{\xi\to-\infty} v(\xi,.) = V_M$ with a negative speed $c < 0$.
ii) If $R_1 < R$ there exists a globally stable travelling front $u(x,y,t) = v(x-ct,y)$ with $\lim_{\xi\to+\infty} v(\xi,.) = 0$ and $\lim_{\xi\to-\infty} v(\xi,.) = V_M$ with a positive speed $c > 0$.

Assertion i) is a clear consequence of Theorem 1.1. The proof that this theorem also implies the other assertions is not the goal of this paper and will not be detailed. One way

to prove it is to use a method recently introduced by Risler in [25]. The fundamental idea is to use the existence of an energy functional for (1.3) in any Galilean frame travelling at constant speed s in the x direction. Keeping this basic idea, the original proof has been revised in [11] and [10]. The adaptation of these techniques to Eq. (1.3) has been detailed in [4]. The original motivation of Risler's techniques was to develop a method of proof of existence and stability of fronts in equations where no comparison principle is available. As suggested by the work of the first author in [4], the method of Risler is also useful to get the existence and stability of fronts in equations as (1.3) for which even if there is a comparison principle, no particular positive subsolution is known.

The results of this article improve our understanding of the different behaviours of the depolarisation in the grey matter after it has been stimulated. If the stimulation takes place in a part of a brain where the grey matter is thin ($R < R_0$), the neurons of the grey matter quickly repolarise, i.e. the solution of (1.3) goes back to zero, uniformly and exponentially fast. If the grey matter is slightly thicker ($R_0 < R < R_1$), the repolarisation is slower and more progressive, the depolarised area disappearing by shrinking. Mathematically speaking, there exists a stable non-trivial profile but with an energy larger than zero. Thus, the equilibrium state zero invades the excited state by travelling fronts, reducing the excited area. Notice that it may take a long time to go back to rest if the initial excited area is large. Finally, if the grey matter is thick ($R_1 < R$), a depolarisation wave propagates. Indeed, the excited state has a lower energy than zero. These three types of behaviour are illustrated in Fig. 1. The dependence of the behaviour on the width of the grey matter may explain why the depolarisation waves have been observed or not in the human brain depending on the experiments, see [1, 18, 19] or [30] and the discussion in Section 6.

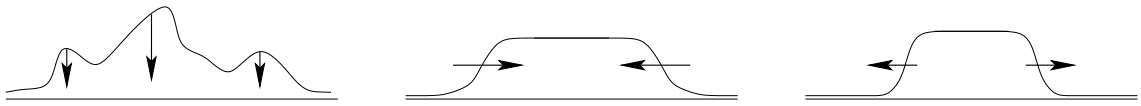

Figure 1: *The three types of behaviour of the depolarisation in the grey matter after stimulation. From left to right: $R < R_0$, going back to rest uniformly; $R_0 < R < R_1$, going back to rest by fronts; $R_1 < R$, invasion by the excited state by fronts.*

Discussion on the interpretations of the main results. We would like to emphasise that (1.1) is an explanatory model rather than a predictive model: the equation has been largely simplified for theoretical analysis in order to isolate the dependence of the qualitative behaviour on the thickness of the layer of grey matter. Mathematical analysis of models such as (1.3) are helpful because in real experiments and numerical simulations it is not possible to eliminate the effects of other parameters. Since this is a simplified model, which has no claim to be predictive, we will not attempt to fit the parameters to data from real biological experiments. In particular, it would probably not be useful to attempt to estimate the critical radii R_0 and R_1, since, even if they were observable, they may depend on others parameters such as the brain curvature or the species. Let us simply recall that many mathematical models of the same type have already been discussed [3, 23, 24, 27, 29, 31]. Numerical proofs of the effect of brain morphology on the

propagation of depolarisation waves have also already been published and these studies have taken into account biological parameter values and geometry [3, 14].

Here, we study the influence of white matter on the propagation of spreading depression. Our goal is to improve our understanding of the influence of the thickness of the grey matter on the qualitative behaviour of spreading depression, and not to yield any quantitative medical information. Our main results show that, even in a simplified model, the variations in thickness of the layer of grey matter may explain by itself why depolarization waves are observed in the human brain in some experiments, and not in others (see Section 6). This paper also highlights the three possible types of behaviour of Fig. 1. Thus, if the modelling is relevant, these types of behaviour should appear in the brain, the thickness of the grey matter layer determining which behaviour can be observed in which location. It is noteworthy that previous numerical studies did not distinguish between the first two types of behaviour because the depolarised area chosen was too small. The introduction of the intermediate case $R_0 < R < R_1$ in the modelling of spreading depressions is one of the main results of this paper. It might be interesting to investigate the medical consequence of the existence of this intermediate behaviour, see Section 6.

The paper is split as follows. In Section 2 a relation between the profiles and the equilibrium points of a parabolic equation in $(-R, R)$ is made explicit. In Section 3, graphic criteria on existence and stability of the profiles are obtained, they are mainly based on Sturm-Liouville theory. The energy of the different profiles is studied in Section 4, using techniques coming from the infinite dimensional dynamical systems theory. Section 5 contains some numerical simulations of the evolution of the depolarisation area and numerical estimates of the critical radii. Finally, in Section 6, relations between the mathematical results and the biological phenomena are discussed.

2 Relations with a parabolic equation on $(-R, R)$

In this preliminary section, we enhance an obvious relation between the profiles solutions of (1.4) and the equilibrium points of a parabolic equation on the segment $(-R, R)$. We also recall some basic properties of the dynamics of this parabolic equation. In fact, in this paper, we could perform all the arguments with the parabolic equation on the whole domain $\mathbb{R}$, but this would bring useless technicalities.

2.1 Back to a bounded interval

The profiles V are the solutions of Eq. (1.4). In other word, they are the stationary solutions of the evolution equation

$$\frac{\partial u}{\partial t} = \frac{\partial^2 u}{\partial y^2} + g(y, u) \tag{2.1}$$

where $g(y,u) = f(u)\mathbb{1}_{|y|\leq R} - \alpha u \mathbb{1}_{|y|>R}$. The energy corresponding to this reaction-diffusion equation is the functional $E : H^1(\mathbb{R}) \longrightarrow \mathbb{R}$ defined by

$$E(u) = \frac{1}{2}\int_{\mathbb{R}} \left|\frac{du}{dy}(y)\right|^2 dy \; - \; \int_{\mathbb{R}} G(y,u(y))dy \tag{2.2}$$

where $G(y,u) = \int_0^u g(y,v)dv$ is a primitive of g.

We notice that any profile V satisfies $V(y) = c_+ e^{\sqrt{\alpha}y} + c_- e^{-\sqrt{\alpha}y}$ outside $(-R,R)$. Since V belongs to $H^2(\mathbb{R})$, one has $c_+ = 0$ for $y > R$ and $c_- = 0$ for $y < R$. Since $H^2(\mathbb{R}) \subset \mathcal{C}^1(\mathbb{R})$, V is continuous and solving (1.4) is equivalent to solving the following problem

$$\left\{ \begin{array}{ll} V''(y) + f(V(y)) = 0 & y \in (-R,R) \\ V'(-R) = \sqrt{\alpha}\, V(-R) & \\ V'(R) = -\sqrt{\alpha}\, V(R)\ . & \end{array} \right. \tag{2.3}$$

Eq. (2.3) characterises the equilibrium points of a parabolic equation on $(-R,R)$ with Robin boundary conditions

$$\left\{ \begin{array}{ll} \dfrac{\partial u}{\partial t}(y,t) = \dfrac{\partial^2 u}{\partial y^2}(y,t) + f(u(y,t)), & (y,t) \in (-R,R)\times\mathbb{R}_+, \\ \dfrac{\partial u}{\partial y}(-R,t) = \sqrt{\alpha}\, u(-R,t), & t > 0, \\ \dfrac{\partial u}{\partial y}(R,t) = -\sqrt{\alpha}\, u(R,t), & t > 0. \end{array} \right. \tag{2.4}$$

The energy corresponding to Eq. (2.4) is given by

$$\mathcal{E}(u) = \frac{1}{2}\int_{-R}^{R} \left|\frac{du}{dy}(y)\right|^2 dy \; - \; \int_{-R}^{R} F(u(y))dy + \frac{\sqrt{\alpha}}{2}\left(|u(R)|^2 + |u(-R)|^2\right) \tag{2.5}$$

where $F(u) = \int_0^u f(v)dv$ is a primitive of f.

It is straightforward to verify that if V is a profile, then $E(V) = \mathcal{E}(V_{|(-R,R)})$. As a conclusion, the problems of the existence and the energy of the profiles are equivalent to the study of the equilibrium points of the parabolic equation (2.4) and their energy. We will often abusively denote $V_{|(R,R)}$ by simply V. However, notice that the dynamics of the equation (2.1) on the whole real line and the ones of (2.4) on $(-R,R)$ are different. Moreover, the spectrum of the linearization of (2.1) at a profile V is different from the spectrum of the linearization of (2.4) at $V_{|(-R,R)}$, even if we prove in Section 3.2 that the number of positive eigenvalues is the same.

2.2 Basic facts about the parabolic equation on $(-R,R)$

The theory of the parabolic equation (2.4) with Robin boundary conditions is very well-known, see for example [16]. We recall here some basic dynamical properties, which will be used in this paper.

First, (2.4) admits a comparison principle.

Lemma 2.1. *Let $u(t)$ and $v(t)$ be two solutions of (2.4) with respective initial data u_0 and v_0 belonging to $H^1(-R,R)$. Assume that $u_0(y) \leq v_0(y)$ for all $y \in (-R,R)$. Then, for all $(y,t) \in (-R,R) \times \mathbb{R}_+$, $u(y,t) \leq v(y,t)$.*

Secondly, the parabolic type of (2.4) and the fact that $f(u)u < 0$ for large u implies that any solution $u(t)$ with initial data $u_0 \in H^1(-R,R)$ is bounded in $H^k(-R,R)$ uniformly for $t \in [t_0, +\infty)$ for any $t_0 > 0$ and for any $k \in \mathbb{N}$. This yields a compactness result.

Lemma 2.2. *Let $(t_n)_{n\in\mathbb{N}}$ be a sequence of times such that $\liminf t_n > 0$, let $(u_n^0)_{n\in\mathbb{N}} \subset H^1(-R,R)$ be a sequence of initial data and let $u_n(t)$ be the solutions of (2.4) with $u_n(0) = u_n^0$.*
Then, there exist an extraction φ and a function $u_\infty \in H^1(-R,R)$ such that $\|u_{\varphi(n)}(t_{\varphi(n)}) - u_\infty\|_{H^1(-R,R)} \longrightarrow 0$ when n goes to $+\infty$.

The energy $\mathcal{E}$ defined by (2.5) is a strict Lyapounov functional for the dynamics of (2.4): for each $u(t) \in H^1(-R,R)$ solution of (2.4), the function $\mathcal{E}(u(t))$ is decreasing in time, except if $u(t)$ is constant, that is except if u is an equilibrium point, and thus a profile. Indeed, it is straightforward to get $\partial_t \mathcal{E}(u(t)) = -\int_{-R}^{R} |\frac{\partial u}{\partial t}(y,t)|^2 dt$. The existence of a strict Lyapounov function yields what are called gradient dynamics. In addition of the compactness property of Lemma 2.2, it is very classical to obtain Lasalle principle, see [15].

Lemma 2.3. *Let $u(t)$, $t \geq 0$, be a solution in $H^1(-R,R)$ of (2.4). Let $\omega(u)$ be the $\omega-$limit set of u, that is*

$$\omega(u) = \left\{ v \in H^1(-R,R) \ / \ \exists (t_n)_{n\in\mathbb{N}},\ t_n \xrightarrow[n\to\infty]{} +\infty \ \text{ and } \ \|u(t_n) - v\|_{H^1(-R,R)} \xrightarrow[n\to\infty]{} 0 \right\} .$$

Then, $\omega(u)$ is a non-empty connected compact set which only consists in equilibrium points, i.e. in profiles.
Similarly, if $u(t)$ is defined for all $t \in \mathbb{R}$ and uniformly bounded, the $\alpha-$limit set

$$\alpha(u) = \left\{ v \in H^1(-R,R) \ / \ \exists (t_n)_{n\in\mathbb{N}},\ t_n \xrightarrow[n\to\infty]{} -\infty \ \text{ and } \ \|u(t_n) - v\|_{H^1(-R,R)} \xrightarrow[n\to\infty]{} 0 \right\}$$

is a non-empty connected compact set which only consists in profiles. Moreover, if u is no equilibrium, if $V_- \in \alpha(u)$ and $V_+ \in \omega(u)$ then $\mathcal{E}(V_-) > \mathcal{E}(V_+)$ and in particular $V_- \not\equiv V_+$.

3 Existence and stability of profiles

3.1 A graphic criterion for existence of profiles

We recall here the simple graphic arguments already mentioned in [4]. We are interested in the asymptotic profiles of the possible travelling fronts of Eq. (1.3), that are solutions $V \in H^1(\mathbb{R})$ of (1.4). As already noticed, looking for profiles V solutions of (1.4) is equivalent to looking for solutions V of the equation (2.3). In the phase plane, the flow

$\Phi_{y_0} : \mathbb{R}^2 \longrightarrow \mathbb{R}^2$ associated to the differential equation $V'' + f(V) = 0$ between $-R$ and y_0 is given by

$$\Phi_{y_0}(V_0, V_1) = (V(y_0), V'(y_0)) \quad \text{where } V \text{ solves} \quad \begin{cases} V''(y) + f(V(y)) = 0\ , \quad y \in (-R, y_0) \\ (V(-R), V'(-R)) = (V_0, V_1) \end{cases}$$

Let $\mathcal{D}$ and $\mathcal{D}' \subset \mathbb{R}^2$ be the straight lines $\mathbb{R}.(1, \sqrt{\alpha})$ and $\mathbb{R}.(1, -\sqrt{\alpha})$. Notice that the conditions $V'(-R) = \sqrt{\alpha}\, V(-R)$ and $V'(R) = -\sqrt{\alpha}\, V(R)$ correspond to $(V, V')(-R) \in \mathcal{D}$ and $(V, V')(R) \in \mathcal{D}'$ respectively. Hence, the graphic interpretation of (2.3) is the following.

Graphic criterion 3.1. *The profiles, i.e. the solutions of* (2.3)*, correspond to the trajectories of the flow Φ_y that start on $\mathcal{D}$ when $y = -R$ and finish on $\mathcal{D}'$ when $y = R$. Therefore, they correspond to the intersections of the curve $\Phi_R\mathcal{D}$ with the straight line $\mathcal{D}'$.*

The results of existence stated in Theorem 1.1 follow from Graphic Criterion 3.1. The critical radius R_0 is the first (positive) R such that $\Phi_R\mathcal{D}$ intersects $\mathcal{D}'$ elsewhere than at $(0, 0)$. In Fig. 2 and 3, we illustrate the phase plane, the flow Φ_y and the curve $\Phi_R\mathcal{D}$ for different cases. Fig. 4 shows the graph of four profiles $V(y)$ in $[-R, R]$ and the corresponding intersections in the phase plane.

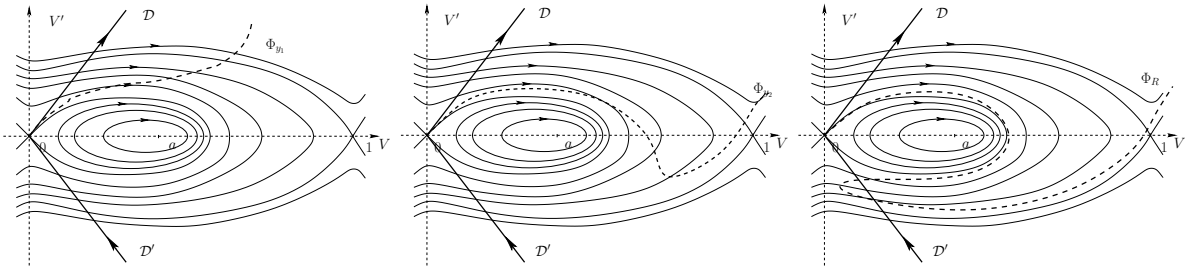

Figure 2: *The phase plane for $\alpha \geq a\lambda$ (solid lines) and $\Phi_R\mathcal{D}$ (dashed line) for three increasing values of R: two cases with no non-trivial profiles and the last with two non-trivial profiles.*

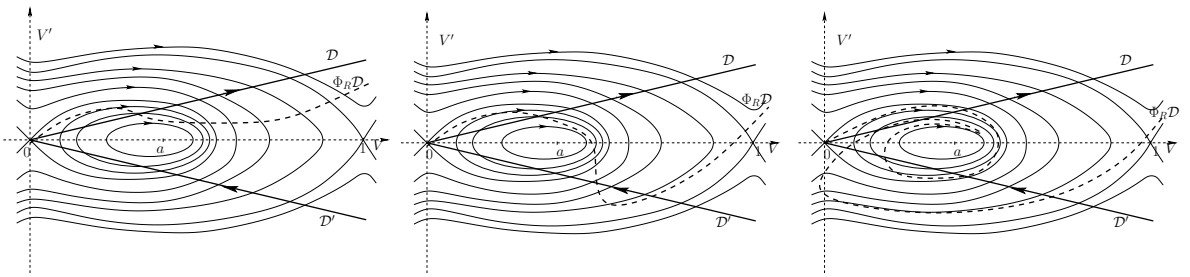

Figure 3: *The phase plane for $\alpha < a\lambda$ (solid lines) and $\Phi_R\mathcal{D}$ (dashed line) for three increasing values of R: no non-trivial profiles, two ones and four ones.*

Fig. 2 and 3 show that there are two cases. If $\mathcal{D}$ is always outside the domain delimited by the homoclinic orbit to zero, then there cannot exist more than two non-trivial profiles.

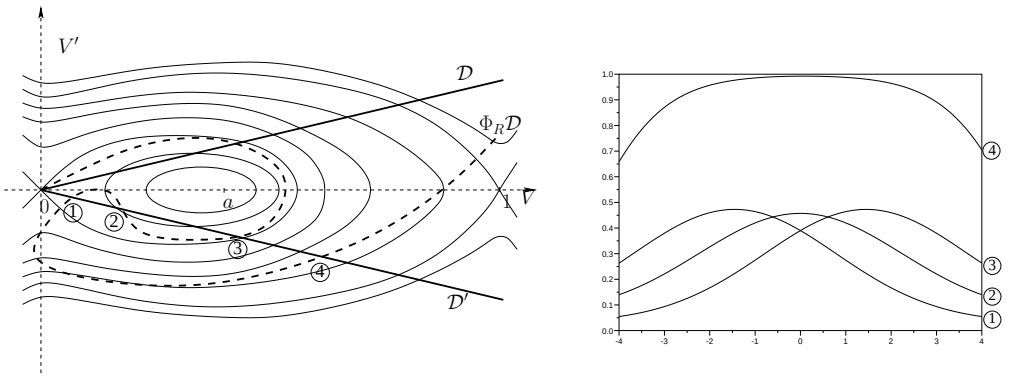

Figure 4: *The intersections of $\Phi_R\mathcal{D}$ and $\mathcal{D}'$ in the phase plane and the corresponding profiles in the (y, V) plane*

If $\mathcal{D}$ intersects the homoclinic orbit to zero, then for R large enough there exist as much non-trivial profiles as may be wanted. The critical value of α is obtained by computing the unstable direction of 0 in the phase plane. This direction is given by the eigenvector $(1, \sqrt{a\lambda})$ related to the eigenvalue $\sqrt{a\lambda}$ of the matrix $\begin{pmatrix} 0 & 1 \\ a\lambda & 0 \end{pmatrix}$, which corresponds to the linearization of the flow at the equilibrium point $(0, 0)$. This shows that $\mathcal{D}$ intersects the homoclinic orbit to zero if and only if $\alpha < a\lambda$.

The fact that there exists a profile V_M larger than the other ones is classical, see for example [26]. It is a consequence of Lemmas 2.1 and 2.3: if $u(t)$ is a solution of (2.4) with $u(0)$ larger than any profile, then the $\omega-$limit set $\omega(u(0))$ consists in a profile V_M larger than any profile. The fact that V_M is even follows from the symmetry of the problem since $V_M(-.)$ is also a profile. Notice that this symmetry corresponds to the symmetry of the phase plane and to the fact that the trajectory $y \mapsto \Phi_y(V_M(-R), V_M'(-R))$ intersect $\mathcal{D}'$ for the first time at $y = R$.

3.2 A graphic criterion for stability of the profiles

Let V be a profile solution of (1.4). We consider the linearization $L_V : H^2(\mathbb{R}) \longrightarrow L^2(\mathbb{R})$ of the flow along the profile V given by

$$L_V\varphi = \varphi'' + \left(f'(V)\mathbb{1}_{|y|\leq R} - \alpha\mathbb{1}_{|y|>R}\right)\varphi \ . \tag{3.1}$$

The operator L_V is self-adjoint and is a relatively compact disturbance of $\Delta-\alpha$ and therefore has the same essential spectrum, see [16]. This yields the following characterisation of the stability of a profile V, see [28].

Proposition 3.2. *The spectrum of L_V consists in $]-\infty, -\alpha]$ and a finite number of isolated real eigenvalues $\mu_i > -\alpha$ of finite multiplicity. As a consequence, the profile V is asymptotically stable if and only if L_V has no non-negative eigenvalue.*

We are looking to non-negative eigenvalues of L_V that is to $\mu \geq 0$ such that there exists $\varphi \in H^2(\mathbb{R})$ such that $\varphi \not\equiv 0$ and

$$\varphi''(y) + \left(f'(V(y))\mathbb{1}_{|y|\leq R} - \alpha\mathbb{1}_{|y|>R}\right)\varphi(y) = \mu\varphi(y) \ . \tag{3.2}$$

By the same argument used for V in Section 2, φ is explicit outside $(-R,R)$ and it is equivalent to look to φ satisfying

$$\left\{\begin{array}{ll}\varphi''(y)+f'(V(y))\varphi(y)=\mu\varphi(y) & y\in(-R,R)\\ \varphi'(-R)=\sqrt{\mu+\alpha}\varphi(-R)\\ \varphi'(R)=-\sqrt{\mu+\alpha}\varphi(R)\end{array}\right. \tag{3.3}$$

In this section, we adapt the standard Sturm-Liouville theory to the eigenvalue problem (3.3), where the eigenvalue μ appears not only in the main equation, but also in the boundary conditions. For any $\mu\geq 0$ we define θ_μ by

$$\left\{\begin{array}{l}\theta'_\mu=-\sin^2\theta_\mu+(\mu-f'(V(y)))\cos^2\theta_\mu \quad , \quad y\in(-R,R)\\ \theta_\mu(-R)=\arctan(\sqrt{\mu+\alpha})\end{array}\right. \tag{3.4}$$

and we set for $\mu>-\alpha$

$$h(\mu)=\theta_\mu(R)+\arctan(\sqrt{\mu+\alpha})\ . \tag{3.5}$$

Lemma 3.3. *A non-negative number μ is a non-negative eigenvalue of L_V if and only if $h(\mu)$ belongs to $\pi\mathbb{Z}$.*

Proof: Let $\mu\geq 0$ and $\varphi\in\mathcal{C}^2([-R,R])$, $\varphi\not\equiv 0$, satisfying (3.3). We introduce two functions of class $\mathcal{C}^2$, $\rho>0$ and $\theta\in\mathbb{R}$, such that $(\varphi,\varphi')(y)=\rho(y)(\cos\theta(y),\sin\theta(y))$. Notice that these functions exist and are regular since the vector (φ,φ') cannot vanish because φ is a non-trivial solution of a linear second-order differential equation. Up to the change of the sign of φ and to the addition of a constant in $\pi\mathbb{Z}$ to θ, $\varphi'(-R)=\sqrt{\mu+\alpha}\varphi(-R)$ implies $\theta(-R)=\arctan(\sqrt{\mu+\alpha})$. Moreover, it follows from (3.3) that, for $y\in(-R,R)$,

$$\begin{array}{l}\theta'=-\sin^2\theta+(\mu-f'(V(y)))\cos^2\theta\\ \rho'=\rho\sin\theta\cos\theta\,(1+\mu-f'(V(y)))\end{array} \tag{3.6}$$

Hence, $\theta=\theta_\mu$ and $\varphi'(R)=-\sqrt{\mu+\alpha}\varphi(R)$ is equivalent to $\theta_\mu=-\arctan(\sqrt{\mu+\alpha})+k\pi$ with $k\in\mathbb{Z}$.
To show the other implication, it is sufficient to follow the previous arguments in the opposite way: we start with a function θ_μ, we construct ρ by (3.6) and we check that $\varphi=\rho\cos\theta_\mu$ is a solution of (3.3). □

Lemma 3.4. *Let V be a profile solution of (1.4).*
i) If $\mu>\|f'(V)\|_\infty$ then, for all $y\in[-R,R]$, $\theta_\mu(y)\in(0,\frac{\pi}{2})$ and $h(\mu)\in(0,\pi)$.
ii) If $\mu_1>\mu_2$ then, for all $y\in[-R,R]$, $\theta_{\mu_1}(y)>\theta_{\mu_2}(y)$ and h is an increasing function.

Proof: We prove assertion i) by contradiction. Let $y_0=\inf\{y\in[-R,R]/\theta_\mu(y)\notin(0,\pi/2)\}$. Notice that $y_0>-R$ since $\theta_\mu(-R)\in(0,\pi/2)$. If $\theta_\mu(y_0)=0$, then $\theta'_\mu(y_0)=\mu-f'(V(y_0))>0$ which is absurd since $\theta_\mu(y)>0$ for $y<y_0$ by definition of y_0. The contradiction is similar if $\theta_\mu(y_0)=\pi/2$.
The proof of ii) is very similar: let $y_0=\inf\{y\in[-R,R]/\theta_{\mu_1}(y)\leq\theta_{\mu_2}(y)\}$. We have $\theta_{\mu_1}(y_0)=\theta_{\mu_2}(y_0)$. If $\theta_{\mu_1}(y_0)\notin\pi/2+\pi\mathbb{Z}$, then $\theta'_{\mu_1}(y_0)-\theta'_{\mu_2}(y_0)=(\mu_1-\mu_2)\cos^2\theta_{\mu_1}(y_0)>0$

and it contradicts the definition of y_0. If $\theta_{\mu_i}(y_0) \in \pi/2 + \pi\mathbb{Z}$, then $\theta'_{\mu_1}(y_0) = \theta'_{\mu_2}(y_0)$, $\theta''_{\mu_1}(y_0) = \theta''_{\mu_2}(y_0)$ and $\theta'''_{\mu_1}(y_0) = 2 + \mu_1 - f'(V(y_0)) > \theta'''_{\mu_2}(y_0)$. In both cases, we obtain the desired contradiction. □

As a consequence of both preceding lemmas, we obtain the following Sturm-Liouville-type result.

Proposition 3.5. *Let V be a profile solution of (1.4). Let L_V be the operator defined by (3.1) and let h be the function defined by (3.5).*
i) The constant $k \in \mathbb{N}$ is such that $h(0) \in (-k\pi, (1-k)\pi]$ if and only if the operator L_V has k non-negative eigenvalues.
ii) If L_V has a non-negative eigenvalue, there exists a positive eigenfunction associated to the largest eigenvalue of L_V.
iii) The non-negative eigenvalues of L_V are simple.

Proof: By Lemma 3.3, the non-negative eigenvalues correspond to the values μ for which $h(\mu) \in \mathbb{Z}$. Since, as shown in Lemma 3.4, $\mu \mapsto h(\mu)$ is increasing and belongs to $(0, \pi)$ for large μ, then Assertion i) follows from the continuity of h. Moreover, if it exists, the largest eigenvalue μ is necessary such that $h(\mu) = 0$. Thus $\theta_\mu(R) \in (-\pi/2, \pi/2)$. Since $\theta_\mu(-R) \in (-\pi/2, \pi/2)$ and since $\theta'_\mu(y) < 0$ as soon as $\theta_\mu(y) = \pm\pi/2$, we must have $\theta_\mu(y) \in (-\pi/2, \pi/2)$ for all $y \in [-R, R]$. Following the arguments in the proof of Lemma 3.3, we construct an associated eigenfunction $\varphi = \rho \cos\theta_\mu$ which is positive on $[-R, R]$. It is positive on $\mathbb{R}$ by the extension imposed by (3.2). Finally, the eigenspace of a non-negative eigenvalue is one-dimensional since any eigenfunction must satisfy (3.3). Since L_V is self-adjoint, any non-negative eigenvalue is simple. □

The interest of the first assertion of Proposition 3.5 is to have a graphic interpretation. Indeed, let φ be the solution of $(\varphi, \varphi')(-R) = (1, \sqrt{\alpha})$ and $\varphi'' + f'(V)\varphi = 0$, i.e. $y \mapsto (\varphi, \varphi')(y)$ is a trajectory of the linearization of the flow $D_V\Phi_y$ along the profile V such that $(\varphi, \varphi')(-R)$ is in the tangent space of $\mathcal{D}$ at $(V, V')(-R)$. For each $y \in (-R, R)$, $(\varphi, \varphi')(y)$ is therefore in the tangent space of $\Phi_y\mathcal{D}$ at $(V, V')(y)$. By the same arguments as in the proof of Lemma 3.3, $\theta_0(y)$ defined by (3.4) is exactly the argument of the vector $(\varphi, \varphi')(y)$. Therefore, one can observe the angle $\theta_0(y)$ by looking at the argument of the vector tangent to $\Phi_y\mathcal{D}$ at $(V, V')(y)$. Thus, we can graphically interpret Assertion i) of Proposition 3.5 in the following way.

Graphic criterion 3.6. *Let V be a profile, solution of (1.4) and let L_V be the operator defined by (3.1). Let $y \in [-R, R] \longmapsto A_V(y) \in \mathbb{R}^2$ be a continuous function such that for all $y \in [-R, R]$, $A_V(y)$ is a unit vector tangent to $\Phi_y\mathcal{D}$ at $(V, V')(y)$. Then, the number of times $A_V(y)$ crosses the direction of $\mathcal{D}'$ when y describes $[-R, R]$ is exactly the number of non-negative eigenvalues of L_V. The crossings have to be counted in a algebraic way: positively in the clockwise sense and negatively otherwise.*

The previous graphic criterion is illustrated in Fig. 5.

This criterion requires the knowledge of the curve $\Phi_y\mathcal{D}$ for each $y \in (-R, R)$. Therefore, it is difficult to apply as it stands. Fortunately, there is a way to count the number

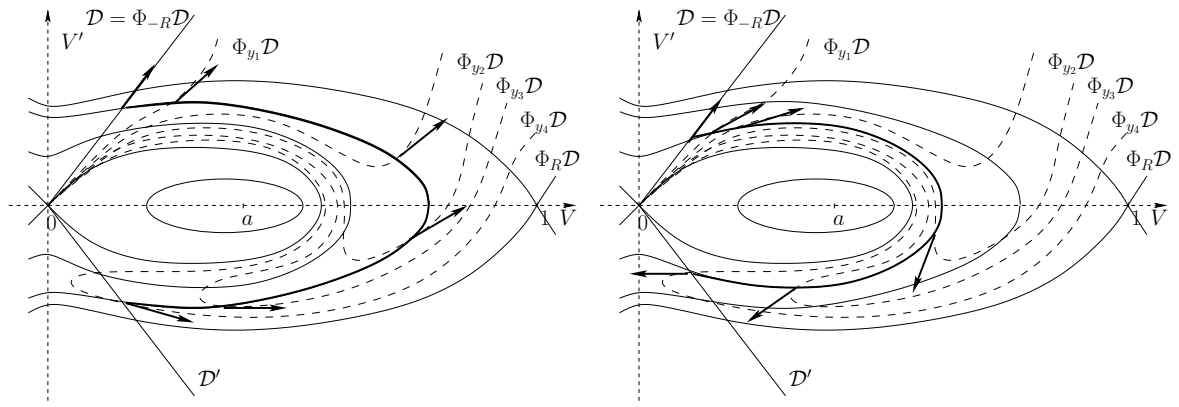

Figure 5: *An example of application of the graphic criterion 3.6. One counts along a profile V the number of crossings between the tangent vector to the curve $\Phi_y\mathcal{D}$ and the direction of $\mathcal{D}'$. This gives the number of nonnegative eigenvalues of L_V. Left, the largest profile has no non-negative eigenvalue. Right, the other non-trivial profile has one non-negative eigenvalue.*

of times $A_V(y)$ crosses the direction of $\mathcal{D}'$ with the knowledge of the curve $\Phi_R\mathcal{D}$ only. Indeed, in the particular case of this article, the phase plane associated to f is such that the curve $\Phi_R\mathcal{D}$ is above $\mathcal{D}'$ in $\{(u,v) \in \mathbb{R}^2,\ u \geq 1\}$ and below $\mathcal{D}'$ in $\{(u,v) \in \mathbb{R}^2,\ u < 0\}$. For this reason, using homotopy and topological arguments, the vectors $A_0(y)$ and $A_{V_M}(y)$ corresponding to the extremal profiles 0 and V_M must have a trivial number of crossings with the direction of $\mathcal{D}'$. Moreover, for another profile V, we can compute the number of crossings of $A_V(y)$ with $\mathcal{D}'$ as follows.

Graphic criterion 3.7. *Let V be a given profile. We follow the curve $\Phi_R\mathcal{D}$ from 0 (or from V_M) to V. We count in a algebraic way the number of times the unit tangent vector to $\Phi_R\mathcal{D}$ crosses the direction of $\mathcal{D}'$ during this course. The resulting number is exactly the number of non-negative eigenvalues corresponding to the profile V.*

The ideas behind the graphic criterion 3.7 are not new, see [9]. The equivalence of the graphic criteria 3.6 and 3.7 can be easily "seen on the figure". However, the rigorous proof uses homotopies and the topology of the plane, similarly to Jordan theorem. This proof is not the subject of this paper and will be omitted.

We can apply the above graphic criterion to the particular phase plane of this article. Because the flow of $V'' + f(V)$ is turning around the equilibrium $(a, 0)$, every profile V, which is not one of the extremal profiles 0 or V_M, is unstable, see Fig. 6. This shows the properties of the stability of the profiles stated in Theorem 1.1.

4 Energy of the profiles

We recall that the relevant energy for the profiles is the function E defined by (2.2). We also recall that the energy $E(V)$ of a profile V is equal to the energy $\mathcal{E}(V_{|(-R,R)})$ of the restriction of V to $(-R, R)$, see Section 2. Let R_0 be the critical thickness introduced

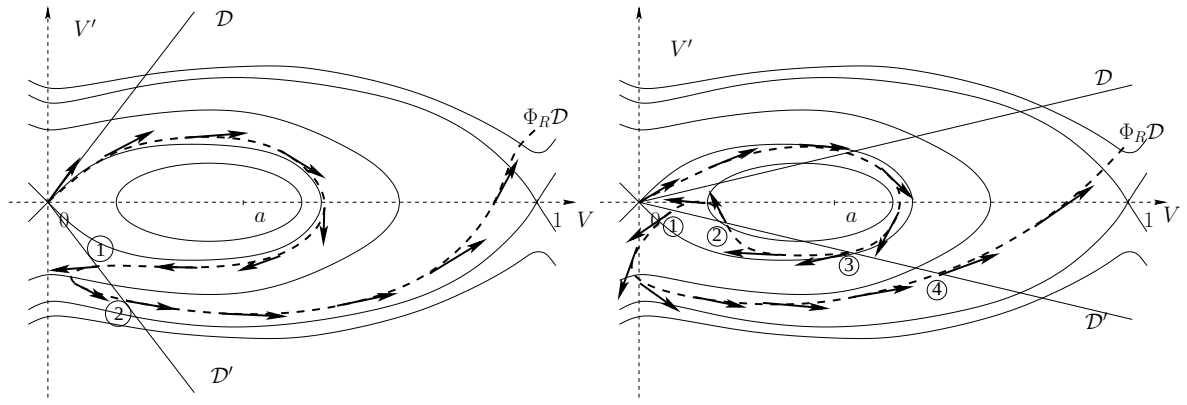

Figure 6: *Examples of application of the graphic criterion 3.7. One follows the curve $\Phi_R\mathcal{D}$ from 0 to a profile V and counts in a algebraic way the number of crossings between the tangent vector to the curve and the direction of $\mathcal{D}'$. One then obtains the number of non-negative eigenvalues of L_V. At the left, the largest profile (2) has no non-negative eigenvalue whereas the other non-trivial profile (1) has one non-negative eigenvalue. At the right, the four non-trivial profiles have respectively one, two, one and zero non-negative eigenvalues.*

in Theorem 1.1. We know that for $R > R_0$ there exists a unique non-trivial profile V_M which is stable and that V_M is the largest profile. This section is devoted to the proof of the following result.

Proposition 4.1.
i) If V is an unstable profile, then $E(V)$ is larger than $E(0) = 0$ and $E(V_M)$.
ii) There exists $R_2 \geq R_0$ such that on (R_0, R_2) (this set being possibly empty, for example if $\alpha \geq a\lambda$) the energy $E(V_M)$ of the largest profile is an increasing function of the radius R and on $(R_2, +\infty)$, $E(V_M)$ is a decreasing function of the radius R.
iii) The energy of the largest profile $E(V_M)$ is positive for $R > R_0$ close to R_0 and converges to $-\infty$ when R goes to $+\infty$.

Proposition 4.1 obviously implies that there exists a radius $R_1 > R_0$ such that $E(V_M)$ is positive for $R_0 < R \leq R_1$ and negative for $R > R_1$, as stated in Theorem 1.1.

4.1 Energy of the unstable profiles

We prove here the first assertion of Proposition 4.1. The proof relies on the following lemma.

Lemma 4.2. *Let V be an unstable profile. Let $\mu > 0$ be the first eigenvalue of L_V and let φ be a positive associated eigenfunction, the existence of which is stated in Proposition 3.5. Then, there exist two globally bounded solutions $u_-(t)$ and $u_+(t)$ of (2.4) with the following prescribed asymptotic behaviour in $H^1(-R, R)$:*

$$u_\pm(t) = V \pm e^{\mu t}\varphi + o\left(e^{\mu t}\right) \quad \text{when } t \longrightarrow -\infty \ . \tag{4.1}$$

As a consequence, for all $(y, t) \in (-R, R) \times \mathbb{R}$, $u_-(y, t) \leq V(y) \leq u_+(y, t)$.

Proof: The lemma is a classical application of the theory of stable and unstable manifolds near an equilibrium point. We refer to [6] and [16]. Indeed, the spectrum of the linearization L_V can be split into $\{\mu\}$ and the spectrum contained in the half-plane $\{z \in \mathcal{C},\ \mathrm{Re}(z) \leq \mu - \varepsilon\}$ with $\varepsilon > 0$ small enough. As shown in Proposition 3.5, μ is simple and admits a positive eigenfunction φ. We defined the strongly unstable set by

$$W^{uu}(V) = \{u_0 \in H^1(-R,R),\ \exists\ u(t) \text{ global solution of (2.4) such that} \\ \lim_{t\to-\infty} e^{(-\mu+\varepsilon/2)t}\|u(t) - V\|_{H^1(-R,R)} = 0\ \}\ .$$

The theory of invariant manifolds near an equilibrium point shows that $W^{uu}(V)$ is an invariant one-dimensional manifold which is tangent at V to the line $V + \mathbb{R}\varphi$. The manifold $W^{uu}(V)$ consists in V and two globally defined trajectories u_+ and u_- satisfying the asymptotic behaviour (4.1). Of course, the last assertion is a direct consequence of this asymptotic behaviour, of the positivity of φ and of Lemma 2.1. □

The first assertion of Proposition 4.1 is deduced from Lemma 4.2 as follows. Let V be an unstable profile. We know from Section 3 that V lies between 0 and the largest profile V_M, both being stable. Let $u_-(t)$ be the solution given by Lemma 4.2 for the profile V. By Lemma 2.2, the $\omega-$limit set of u_- is non-empty and consists in profiles. We wonder which profiles may belong to this $\omega-$limit set. Assume that there is an unstable profile $\tilde{V}$ in $\omega(u_-)$. This profile must satisfy $\tilde{V} \leq V$ since $u_-(t) \leq V$ for all t. Moreover, by Lemma 2.3, $\tilde{V} \not\equiv V$ and thus, by uniqueness of ODE solutions, $\tilde{V}(y) < V(y)$ for all $y \in \mathbb{R}$. Let $\tilde{u}_+(t)$ be the solution given by Lemma 4.2 for the profile $\tilde{V}$. For t close to $-\infty$, $\tilde{u}_+(t) < u_-(t)$. Using Lemma 2.1, $\tilde{V} \leq \tilde{u}_+(t) \leq u_-(t) \leq V$ for all times. Since Lemma 2.3 prevents $\tilde{u}_+(t)$ to go back to $\tilde{V}$, $u_-(t)$ cannot converge to $\tilde{V}$, which yields a contradiction. Therefore, since $\omega(u_-)$ is non-empty, the only possibility is $\omega(u_-) = \{0\}$. Lemma 2.3 then shows that $E(V) = \mathcal{E}(V) > \mathcal{E}(0) = E(V) = 0$.

By using $u_+(t)$, we prove similarly that $E(V) = \mathcal{E}(V) > \mathcal{E}(V_M) = E(V_M)$. Notice that the above arguments also prove that every unstable profile intersects the other unstable ones as illustrated in Fig. 4.

4.2 Energy of the stable profile

The proof of the second and third assertions of Proposition 4.1 is split in several parts. We use in this section the notations of Section 3.1 with a superscript R to point out the dependence of the different objects with respect to R.

• $R \mapsto V_M^R(0)$ **is increasing.**
To study the function $R \mapsto V_M^R$, we invoke the graphic interpretation of the profiles developed in Section 3.1. By symmetry of the largest profile, $V_M^R(0)$ is the intersection of the trajectory $y \mapsto \Phi_y(V_M^R(-R), \sqrt{\alpha}V_M^R(-R))$ with the horizontal axis. Therefore, $R \mapsto V_M^R(0)$ is increasing if and only if $R \mapsto V_M^R(-R)$ is increasing. For R given, $\Phi_R(V_M^R(-R), \alpha V_M^R(-R))$ belongs to $\mathcal{D}'$ and at this point of the phase plane, the flow Φ_y crosses $\mathcal{D}'$ transversely from the top to the bottom. Thus, for small $\varepsilon > 0$, $\Phi_{R+\varepsilon}(V_M^R(-R), \alpha V_M^R(-R))$ is below $\mathcal{D}'$ and by continuity, there exists an intersection of $\Phi_{R+\varepsilon}\mathcal{D}$ and $\mathcal{D}'$ at the right

of $\Phi_{R+\varepsilon}(V_M^R(-R), \alpha V_M^R(-R))$. This means that $V_M^{R+\varepsilon}(-R-\varepsilon) > V_M^R(-R)$ and thus $R \mapsto V_M^R(0)$ is increasing. See Fig. 7.

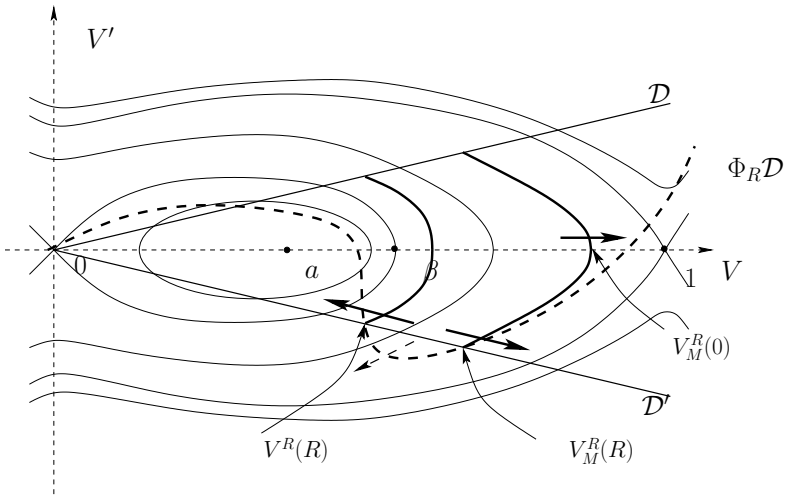

Figure 7: *When $R = R_0$, a saddle-node bifurcation creates a stable profile V_M^R (the largest profile) and an unstable profile V^R. When $R > R_0$ increases, the largest profile V_M^R is increasing. When $R \to +\infty$ the largest profile V_M^R piles up to the singularity $(1, 0)$ of the phase plane.*

By a standard implicit functions argument, one shows that $R \mapsto V_M^R$ is continuous and differentiable as soon as $\Phi_R\mathcal{D}$ intersects $\mathcal{D}'$ transversely at $(V_M^R(R), -\sqrt{\alpha}V_M^R(R))$. We admit that it is always the case when $R > R_0$.

• $E(V_M^R)$ **converges to** $-\infty$ **when** R **goes to** $+\infty$**.**
This fact has already been proved in [4] by the first author. We only give here brief arguments. When R increases, the trajectory $y \in (-R, R) \mapsto \Phi_y(V_M^R(-R), \sqrt{\alpha}V_M^R(-R))$ goes to the right and $V_M^R(0)$ converges to 1. For large R, the trajectory $y \in (-R, R) \mapsto \Phi_y(V_M^R(-R), \sqrt{\alpha}V_M^R(-R))$ spends a time $O(R)$ in a neighbourhood of $(1, 0)$, where $(u, v) \mapsto \frac{1}{2}|v|^2 - F(u)$ is negative, and a bounded time outside. Therefore $E(V_M^R) = \mathcal{E}(V_M^R)$ goes to $-\infty$ when R goes to $+\infty$.

• **There exists** $\beta \in (a, 1)$ **such that** $R \mapsto E_R(V_M^R)$ **is increasing if** $V_M^R(0) < \beta$ **and decreasing if** $V_M^R(0) > \beta$
We admit that for all $R > R_0$, $R \mapsto V_M^R(y)$ is differentiable. Let E_ρ be the energy functional defined by (2.2) with $R = \rho$. Let V be a given fixed profile. We consider the variation of $\rho \mapsto E_\rho(V)$ at $\rho = R$.

$$\partial_\rho E_\rho(V)_{|\rho=R} = \left(-F(V(R)) - \frac{\alpha}{2}|V(R)|^2\right) + \left(-F(V(-R)) - \frac{\alpha}{2}|V(-R)|^2\right)$$

Since $V(\pm R) = \pm\sqrt{\alpha}\, V'(\pm R)$ and since $V''(y) + f(V(y)) = 0$, $y \mapsto \frac{1}{2}|\partial_y V(y)|^2 + F(V(y))$ is constant and

$$\partial_\rho E_\rho(V) = -2F(V(0)) \ .$$

Since V is an equilibrium of (2.1), it is a critical point for the energy E_R. In other words, for any $W \in H^1(\mathbb{R})$,

$$\partial_h \left[E_R(V + hW)\right](0) = 0 \ .$$

Henceforth, if $R \mapsto V_M^R$ is differentiable, then combining both derivatives yields

$$\partial_R \left(E_R(V_M^R) \right) = -2F(V_M^R(0)) \ .$$

It remains to notice that $R \mapsto V_M^R(0)$ is increasing and converges to 1 when R goes to $+\infty$. Moreover, there exists $\beta > 0$ such that F is negative on $(0, \beta)$ and positive on $(\beta, 1]$. In fact, $(\beta, 0)$ is the point of the phase plane where the homoclinic orbit to 0 intersects the horizontal axis, see Fig. 7.

• $E_R(V_M^R)$ **is positive for** R **close to** R_0**.**

When R passes the value R_0, the creation of both non trivial profiles occurs through a saddle-node bifurcation: two equilibrium states appear at the same point, one stable and one unstable. The stable profile is V_M^R, the largest one, and we denote by V^R the unstable profile which lies between 0 and V_M^R. From now on, we work in $(-R, R)$ by using the analogy presented in Section 2. We want to show that $\mathcal{E}(V_M^R)$ is positive for R close to R_0. When R decreases to R_0: the profiles V_M^R and V^R collide. As $\mathcal{E}(V^R) > 0$ for $R > R_0$ as shown in Section 4.1, we must have at the limit $\mathcal{E}(V^{R_0}) = \mathcal{E}(V_M^{R_0}) \geq 0$. Assume that $\mathcal{E}(V_M^{R_0}) = 0$. Let $R_n > R_0$ be a sequence of thickness decreasing to R_0 and let V^{R_n} be the associated unstable profiles. Let $u_-^n(t)$ be the sequence of solutions of (2.4) given by Lemma 4.2 applied to V^{R_n}. We know by Section 4.1 that $u_-^n(t)$ converges to 0 when t goes to $+\infty$. Let $K = \lim_{n\to+\infty} \|V^{R_n}\|_{H^1(-R,R)}$. Notice that K is positive since for each n there exists $y \in (-R, R)$ such that $V^{R_n}(y) > a$. We set t_n to be a time such that $\|u_-^n(t_n)\|_{H^1(-R,R)} = K/2$. By a compactness argument similar to Lemma 2.2 (R is moving, but nothing singular happens), one can extract a subsequence such that $u_-^{\varphi(n)}(t_{\varphi(n)})$ converges in $H^1(-R, R)$ to a function u^∞. Notice that by construction, u^∞ is neither 0 nor V^{R_0}. The gradient structure of (2.4) shows that, for all n and t, $0 < \mathcal{E}(u_-^n(t)) < \mathcal{E}(V^{R_n})$ and thus $\mathcal{E}(u^\infty) = 0$. Let $u^\infty(t)$ be the solution of (2.4) for $R = R_0$, with initial data u^∞. This solution is not a profile, and so its energy $\mathcal{E}(u(t))$ decreases and is negative for $t > 0$. However, $u^\infty(t)$ must converge to a profile when t goes to $+\infty$ due to Lemma 2.3. Since all the profiles at $R = R_0$ have an energy equal to 0 by assumption, this is impossible and we get a contradiction. Therefore, $\mathcal{E}(V^{R_0}) = \mathcal{E}(V_M^{R_0}) = E(V_M^{R_0})$ must be positive and the proof of Proposition 4.1 is over.

5 Some numerical simulations

The three different types of behaviour of the depolarisation area after stimulation are highlighted by the numerical simulations of Fig. 8. Notice that the difference between $R < R_0$ and $R_0 < R < R_1$ can be clearly seen as soon as the initial excited area is large enough.

An interesting point is to estimate the critical radii R_0 and R_1 as a function of the different parameters λ, a and α in order to check if the intermediate case $R_0 < R < R_1$ appears in a significant range of parameters and if the dependence with respect to the parameters agrees with the expected one. Since the parameter values of our model are chosen arbitrarily, these radii could only be expressed in arbitrary units. Moreover, we recall that Eq. (1.3) is an explanatory model introduced to study the qualitative behaviour of spreading depression. It has no claim to be predictive or to provide any quantitative

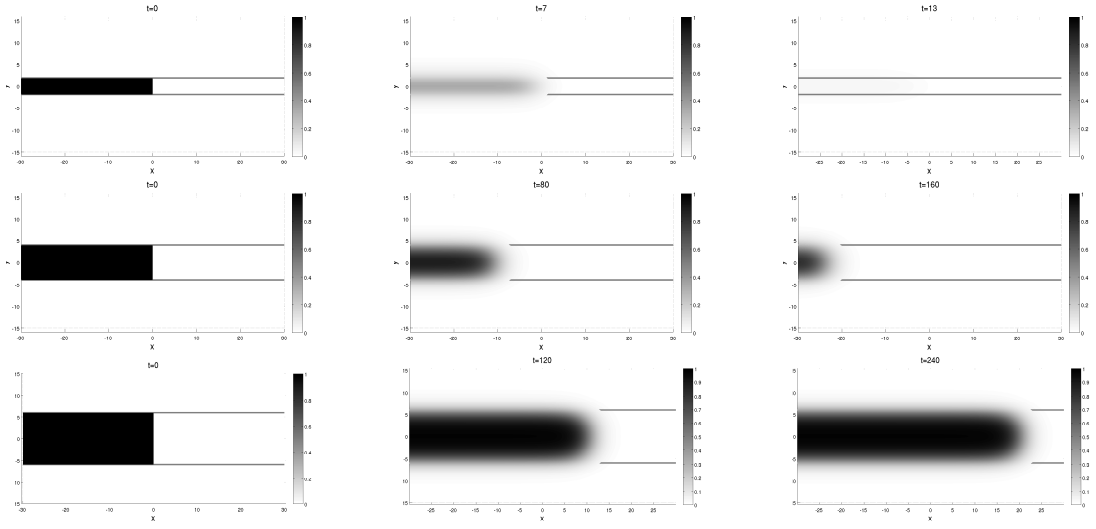

Figure 8: *Numerical simulations of the excited area. The reference parameter values are* $\lambda = 1$, $a = 0.3$ *and* $\alpha = 0.6$*; time is increasing from left to right; the depolarisation is the strongest in the black area. From top to bottom, the thickness of the layer of grey matter is increasing:* $R = 2 < R_0$ *the grey matter goes back to rest uniformly,* $R_0 < R = 4 < R_1$ *the grey matter goes back to rest by a front and* $R_1 < R = 5.5$ *the depolarisation propagates.*

information. Thus, it is unnecessary to attach too much importance to estimating the biological values of λ, a and α and using numerical simulations to deduce the values of the critical radii in a biological setting.

In order to compute the radius R_0 above which there exists at least one non-zero asymptotic profile, we have used a dichotomy algorithm and to decide if $R > R_0$ or $R \leq R_0$, we have used a "shooting method". Precisely, we have approached the solution of

$$\begin{cases} u'' + f(u) = 0 \quad \text{on }]-R, R[\\ u(-R) = s > 0,\ u'(-R) = \sqrt{\alpha} s, \end{cases}$$

with the `ode45` Matlab function (a Runge-Kutta method of order 4 with an adaptive time step) and we have looked for solutions such that $\sqrt{\alpha}u(R) + u'(R) = 0$. In fact, to conclude that $R \geq R_0$, it is enough to find $s > 0$ such that $\sqrt{\alpha}u(R) + u'(R) \leq 0$.

The computation of the radius R_1 once again uses a dichotomy algorithm but it is more delicate to determine if $R > R_1$ (i.e. the energy of the largest asymptotic profile is positive) or if $R \leq R_1$. Indeed the first natural idea is to compute directly the energy of the asymptotic profile using the approximation of the profile obtained with the shooting method. The problem is that errors on the computation of the profile induce large errors on the computation of the energy. Hence, we have preferred to compute the solution of the parabolic problem

$$\begin{cases} \partial_t u - \Delta u = f(u)\mathbb{1}_{|y|<R} - \alpha \mathbb{1}_{|y|\geq R} \\ u(t=0) = \mathbb{1}_{|y|<R}\mathbb{1}_{x\leq 0} \end{cases}$$

on a large box with a semi-implicit finite differences method, as made in Fig. 8. Then,

we have checked if the front propagates to the right (the non-zero profile has a negative energy) or to the left (the non-zero profile has a positive energy).

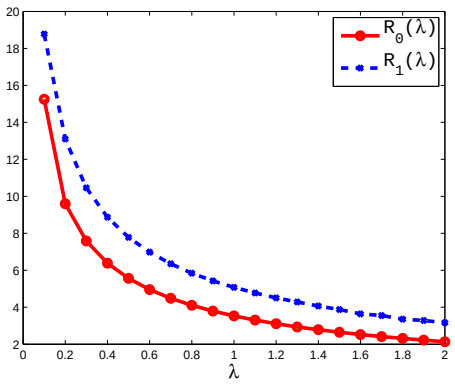

(a) The radii as a function of λ.

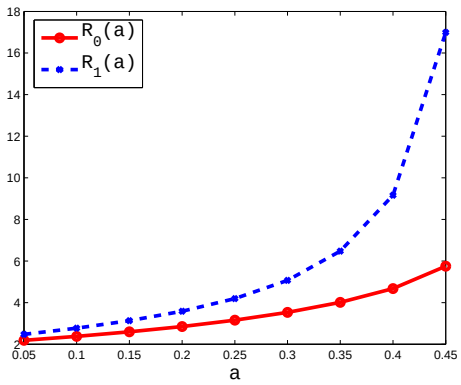

(b) The radii as a function of a.

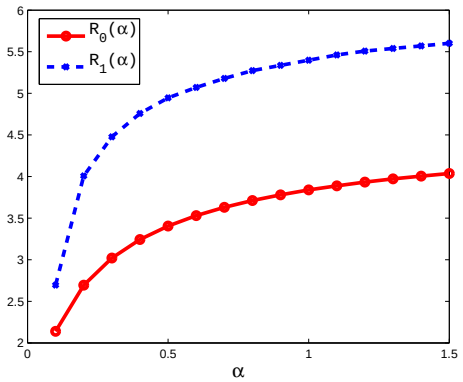

(c) The radii as a function of α.

Figure 9: *Variations of the critical radii R_0 and R_1 as a function of the various parameters of the equation. The other parameters have the reference value ($\lambda = 1$, $a = 0.3$ and $\alpha = 0.6$). The radius R_0 is computed with an accuracy of 0.01 and the radius R_1 with an accuracy of 0.1. Units are arbitrary.*

In Fig. 9, we present the results for the computations of the critical radii according to the parameters of the model (1.1), i.e. λ, a and α. It is noteworthy that the intermediate case $R_0 < R < R_1$, the existence of which has been neglected until now, occurs in a range of parameters which is not so small. Notice that the graphs of Fig. 9 agree with the expected variations of the critical radii: R_0 and R_1 decrease when the diffusion λ increases, they blow up when a goes to 0.5 and, when α goes to $+\infty$, they converges to asymptotic values corresponding to replacing the white matter domain by Dirichlet homogeneous conditions on the boundary of the grey matter domain.

6 Discussion

In this paper, we have proved that there exist two critical thicknesses $R_1 > R_0 > 0$ such that if $0 < R < R_0$, there is no non-trivial profile solution of (1.4). If $R_0 < R$, there exist non-trivial profiles. One of them is larger than every other one and is stable, whereas every other non-trivial profiles are unstable. Finally, the energy of the unstable profiles is always larger than the energy of the stable profiles. If $R_0 < R < R_1$, the energy of the largest profile is larger than the energy of 0, whereas it is smaller if $R > R_1$. These results give us information on the propagation of travelling fronts solution of Eq. (1.1) as stated in Consequence 1.2.

We recall that in Eq. (1.1), u represents the depolarisation of the brain so if $u(X) = 0$ the brain is normally polarised at the point X, and if $u(X) = 1$ the brain is totally depolarised. A depolarisation wave in the brain corresponds to a travelling front solution of (1.1) where a non-trivial stable profile invades the zero state. Thus, the above mathematical analysis of the stability and energy of the asymptotic profiles of equation (1.4) yields information on the propagation of depolarisation waves in the human brain during stroke. Of course Eq. (1.1) is far from being a complete model for an organ as complex as the brain. But its simplicity eliminates the influence of all the parameters but the thickness of the layer of grey matter. It shows that the difficulties to observe depolarisation waves in the human brain could be explained only by the variation of this thickness: if the initial depolarisation takes place in a part of the brain where the grey matter is thick enough, then the depolarisation can spread through a part of the grey matter; if the initial depolarisation takes place in a part of the brain where the grey matter is very thin then no propagation will occur. In the human brain, the grey matter is particularly thin and its thickness may vary a lot. This may explain why attempts to observe depolarisation waves in the human brain have received opposite conclusions in different studies: it is possible to observe depolarisation waves in the human brain [1, 18, 19], but they will not appear in all the cases [29, 30]. Moreover, if a depolarisation wave meets a part of the brain, where the grey matter is too thin, it should stop travelling. Moreover, the brain curvature will increase or decrease the absorbing effect of the white matter depending on the direction of the curve [22, 14]. It is noteworthy that the decrease of the width of the grey matter combined with the curvature of the grey matter may explain by itself why the aura during migraine with aura, which may be due to a depolarisation wave [12, 13], stops for most of the patients at the bottom of the Rolando sulkus which is one of the largest sulkus of the brain and where the grey matter is thin [14].

This paper also gives information on how the initial depolarisation is erased as illustrated in Fig. 1 and 8. If the grey matter is very thin, then the depolarisation is quickly absorbed and uniformly in the excited area. If the grey matter is a little bit larger, the repolarisation occurs in a different way. The depolarised area shrinks progressively while the cells stay totally depolarised as long as they are in the middle of the excited area. In this case, the repolarisation is due to a travelling front where the normally polarised state invades the depolarised state. The neurons in the centre of the excited area may stay depolarised a long time, which may cause local damages even if no spreading wave is observed. To our knowledge this behaviour has never been observed in experiments, but this could be due to a poor space accuracy of measuring instruments. It should also be interesting to study numerically the existence of this intermediate case in a grey matter

layer with more complex geometry.

It seems difficult to estimate the critical radii R_0 and R_1 by knowing the biological parameters of a brain and by computing the corresponding parameters λ, a and α of (1.1). Even the direct measurement of the critical radii for the human brain is a difficult task. Indeed, obtaining such values requires biological experiments in the human white and grey matters of the brain. We recall that even if the mechanisms are the same in the rodent brain and in the human brain, the densities of cells and of transporter on the membrane of those cells are totally different and this clearly influence the values of the parameters of this model and thus the ones of the thresholds. Experiments on human are very difficult to conduct, hence the estimation of biological parameter values would require an entire paper dedicated to the subject.

Acknowledgements: the authors would like to thank Thierry Gallay for several fruitful discussions and the referee, whose remarks lead to a large improvement of this paper.

References

[1] P.G. Aitken, J. Jing, J. Young, A. Friedman, G.G. Somjen, *Spreading depression in human hippocampal tissue in vitro*, Third IBRO Congr. Montreal Abstr. (1991), pp. 329-338.

[2] N. Chafee and E.F. Infante, *Bifurcation and stability for a nonlinear parabolic partial differential equation*, Bulletin of the American Mathematical Society n°80 (1974), pp. 49-52.

[3] G. Chapuisat, *Discussion of a simple model of spreading depression*, ESAIM: Proceedings n°18 (2007), pp. 87-98.

[4] G. Chapuisat, *Existence and non-existence of curved front solution of a biological equation*, Journal of Differential Equations n°236 (2007), pp. 237-279.

[5] G. Chapuisat and E. Grenier, *Existence and nonexistence of travelling wave solutions for a bistable reaction-diffusion equation in an infinite cylinder whose diameter is suddenly increased*, Communications in Partial Differential Equations n°30 (2005), pp. 1805-1816.

[6] X.Y. Chen, J.K. Hale and B. Tan, *Invariant foliations for C^1 semigroups in Banach spaces*, Journal of Differential Equations n°139 (1997), pp. 283-318.

[7] B. Fiedler and C. Rocha, *Heteroclinic orbits of semilinear parabolic equations*, Journal of Differential Equations n°125 (1996), pp. 239-281.

[8] B. Fiedler and A. Scheel, *Spatio-temporal dynamics of reaction-diffusion patterns*, Trends in nonlinear analysis, pp. 23-152, Springer, Berlin, 2003.

[9] G. Fusco and C. Rocha, *A permutation related to the dynamics of a scalar parabolic PDE*, Journal of Differential Equations n°91 (1991), pp. 111-137.

[10] Th. Gallay and R. Joly, *Global stability of travelling fronts for a damped wave equation with bistable nonlinearity*, Annales Scientifiques de l'Ecole Normale Supérieure n°42 (2009), pp. 103-140.

[11] Th. Gallay and E. Risler, *A variational proof of global stability for bistable travelling waves*, Differential and Integral Equations n°20 (2007), pp. 901-926.

[12] A. Gorji, *Spreading depression: a review of the clinical relevance*, Brain Research Reviews n°38 (2001), pp. 33-60.

[13] M. James et al, *Cortical spreading depression and migraine: new insights from imaging?* Trends in neurosciences n°24 (2001), pp. 266-271.

[14] E. Grenier, M.A. Dronne, S. Descombes, H. Gilquin, A. Jaillard, M. Hommel, J.-P. Boissel. A numerical study of the blocking of migraine by Rolando sulcus. Progress in Biophisics and Molecular Biology 2008, 97(1), 54-59.

[15] J.K. Hale, *Asymptotic behavior of dissipative systems*, Mathematical Survey n°25, American Mathematical Society, 1988.

[16] D. Henry, *Geometric theory of semilinear parabolic equations*, Lecture Notes in Mathematics n°840, Springer, Berlin, 1981.

[17] A.A.P. Leão, *Spreading depression of activity in the cerebral cortex*, J Neurophysiol. n°10 (1944), pp. 359-390.

[18] A. Mayevsky, A. Doron, T. Manor, S. Meilin, N. Zarchin, G.E. Ouaknine, *Cortical spreading depression recorded from the human brain using a multiparametric monitoring system*, Brain Res. n°740 (1996), pp. 268-274.

[19] R.S. MacLachlan, J.P. Girvin, *Spreading depression of Leao in rodent and human cortex*, Brain Res. n°666 (1994), p 133-136.

[20] G. Mies, T. Iijima, K.A. Hossman, *Correlation between peri-infarct DC shifts and ischaemic neuronal damage in rat*, Neuroreport n°4 (1993), pp. 709-711.

[21] A.S. Obeidat, C.R. Jarvis, R.D. Andrew. *Glutamate does not mediate acute neuronal damage after spreading depression induced by O2/glucose deprivation in the hippocampal slice*, J. Cereb. Blood Flow & Metab. n°20 (2000), pp. 412-422.

[22] C. Pocci, A. Moussa, F. Hubert and G. Chapuisat, *Numerical study of the stopping of aura during migraine*, ESAIM: Proceedings, to appear (2010).

[23] J.A. Reggia and D. Montgomery, *A computational model of visual hallucinations in migraine*, Comput. Biol. Med. n°26 (1996), pp. 133-139.

[24] K. Revett, E. Ruppin, S. Goodall, J.A. Reggia, *Spreading depression in focal ischemia: a computational study*, J. Cereb. Blood Flow & Metab. n°18 (1998), pp. 998-1007.

[25] E. Risler, *Global convergence towards traveling fronts in nonlinear parabolic systems with a gradient structure*, Annales de l'Institut Henri Poincaré n°25 (2008), pp. 381-424.

[26] A. Rodríguez-Bernal and A. Vidal-López, *Extremal equilibria for reaction-diffusion equations in bounded domains and applications*, Journal of Differential Equations n°244 (2008), pp. 2983-3030.

[27] B.E. Shapiro, *Osmotic forces and gap junctions in spreading depression: a computational model*, Journal of Computational Neuroscience n°10 (2001), pp. 99-120.

[28] J. Smoller, *Shock waves and reaction-diffusion equations*, 2nd Edition. Grundlehren der Mathematischen Wissenschaften, Springer-Verlag:New-York, 1994.

[29] G. Somjen, *Ions in the brain: Normal Function, Seizures, and Stroke.* Oxford University Press: New-York, 2004.

[30] M. Sramka, G. Brozek, J. Buress, P. Nadvornik, *Functional ablation by spreading depression: possible use in human stereptactic surgery*, Appl. Neurophysiol. n°40 (1977), pp. 48-61.

[31] H.C. Tuckwell and R.M. Miura, *A mathematical model for spreading cortical depression*, Biophysical Journal n°23 (1978), pp. 257-276.

[32] J.J. Wylie and R.M. Miura, *Traveling waves in coupled reaction-diffusion models with degenerate sources*, Phys. Rev. E (3) n°74 (2) (2006), 021909, 13 pp.